

μ AUV² - Development of a Minuscule Autonomous Underwater Vehicle

Hendrik Hanff^{1,*}, Korbinian Schmid^{2,*}, Philipp Kloss¹ and Sven Kroffke¹

¹DFKI GmbH – Robotics Innovation Center Bremen, Robert-Hooke Str. 1, 28359 Bremen, Germany

²RoboCeption GmbH, Kaflerstr. 2, 81241 Munich, Germany

Keywords: Underwater Robotics, System Design, Miniature Robotics, System Parameter Identification, Control of Underwater Robots, Robot Development.

Abstract: Small sized robotic systems have operational advantages compared to large systems. They can also operate in fields of application where bigger systems would fail. This paper describes the specifications and the design of the autonomous underwater vehicle μ AUV². Technical details of the system regarding sensor setup, motorization and computing power are given. Furthermore, we present details about the system identification process and the implemented controller structure. Possible scopes of the μ AUV² are underwater exploration, inspection tasks, development and evaluation of algorithms, education and competitions.

1 INTRODUCTION

Autonomous underwater vehicles (AUVs) are robotic systems which do not depend on any input from an operator. Typical fields of application include commercial uses e.g. in the oil and gas industry (Albiez et al., 2015) or the inspection of different underwater structures, research purposes like the autonomous investigation of the ice ocean interface, (Dowdeswell et al., 2008) or even military purposes (Nicholson and Healey, 2008) like autonomous surveillance tasks. The development of AUVs is of great interest to all above mentioned groups. Possible benefits range from monetary advantages to extended capabilities due to the extended range of operation.

Dimensions of AUVs range from small, portable and lightweight to large systems with several meters length. Large systems offer advantages concerning payload capacity, range of operation and the ability to operate when exposed to water currents. In contrast, small systems offer significant advantages during the launch and recovery process due to their small footprint. With their comparably low production and service costs, such systems could even be used as disposable sensor units in situations where a recovery is not possible. Despite these advantages, there only exists a few small and even less minuscule AUVs. The small dimensions enable fields of applications where bigger AUVs would fail. One domain might be the ex-

ploration of underwater cave systems or archaeological sites which are too small or too fragile for normal sized AUVs. Pipeline or wreck inspection could also be addressed by systems like the presented μ AUV² (see Figure 1) or similar systems. Swarms can be realized more easily due to the potentially lower costs per system. The described system is based on knowledge from previous projects and the experiences gained with the μ AUV 1 (Fechner et al., 2007) which can be regarded as the predecessor of the μ AUV².

The μ AUV², developed at the German Research Centre for Artificial Intelligence (DFKI), combines small dimensions ($270 \times 182 \times 156 \text{ mm}^3$ (LxHxW)), a weight of 1.2kg and a maximum speed of 1.5m/s with a unique propulsion concept, and high processing power. This paper presents the system design and development, the identification of system parameters and first control approaches.

The main objectives of the μ AUV² are the development of control and autonomy algorithms. Furthermore the μ AUV² represents an easy to use evaluation platform for swarm algorithms in the underwater area.

2 STATE OF THE ART

In this section, we give an overview of state-of-the-art AUVs and their unique features which inspired the development of the μ AUV². A small form factor, an interesting sensor setup and a streamlined hull are just

**These authors contributed equally to this work.*

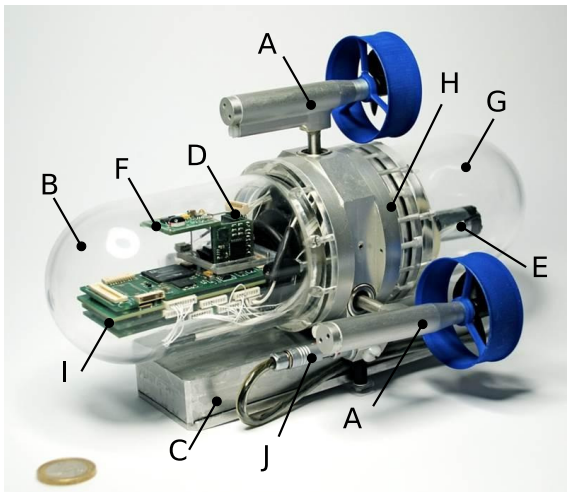


Figure 1: μ AUV² - A: DC motor (Maxon motor with integrated encoder and gear) driven thruster, blue are the 3D printed protection frames, each of the three thrusters can be turned $\pm 90^\circ$, 3rd thruster cannot be seen in this picture; B: Front sphere made from acrylic glass; C: battery pack mounted below the AUV for easy trimming and a low centre of mass (CM); D: IMU, developed at DFKI GmbH, E: peristaltic (buoyancy) pump, a commercially available product; F: Optical communication platform; G: Rear sphere made from acrylic glass; H: Central piece of aluminium which connects the acrylic spheres and serves as a mounting point for the three thrusters and the battery pack; I: Printed Circuit Board (PCB) stack (Microcon1..5) ; J: Connector for the battery pack. Hidden on the other side of the AUV is the JTAG connector which permits reprogramming the FPGA without opening the hull.

some of these features.

The CoCoRo project (Mintchev et al., 2014) has developed the autonomous underwater vehicles Jeff and Lily which interact with each other. Each of the two AUVs fullfills a different task in a swarm. The 3 degrees of freedom (DOF) Jeff system contains custom magnetically coupled thrusters and a custom designed rolling diaphragm buoyancy system. A blue-light sensor system for short-range distance measurement and short-range communication enables the Lily AUV to fullfill swarm operations.

Another example of a small AUV is Monsun (Meyer et al., 2014). Monsun is a small and inexpensive AUV. Just like CoCoRo, Monsun was designed to operate in a swarm. Being equipped with an accelerometer, IMU, compass and a camera makes it ideal for environmental monitoring. Running Linux and ROS on an ARM based microcontroller provides a lot of possibilities concerning camera vision. 6 thrusters enable the system to accelerate in all directions.

Stingray (Barngrover et al., 2011) is a 6 DOF system and was developed by the San Diego iBotics

group. It consists of a carbon fibre hull which mimics the shape of the cartilaginous fish. The streamlined shape enables the underwater vehicle to maneuver very energy efficient. In contrast to other small AUVs, this system makes use of two Voith-Schneider propellers which make this AUV highly agile. The PC-104 form factor computer from Kontron comprises an Intel Core Duo (1.2GHz) with 2Gb of DDR2 RAM and 100Mbps Ethernet. Being equipped with a camera and a low-cost sonar, the Stingray system is able to detect underwater objects.

3 SYSTEM DESIGN

Designing a minuscule underwater vehicle poses hard challenges since commercial of the shelf components (COTS) do generally not meet the design objectives mentioned in the introduction. Therefore, hardware components, electronics as well as mechanics have to be miniaturized. The system has to provide sufficient computational power on strictly limited space, thermal and power constraints. Sensors such as cameras have to be mounted in a way that the acquired data can be used for navigation as well as inspection tasks. Electronics has to be protected from water while fast reprogramming should be possible in a fully assembled state. In the following we describe our system design considering these aforementioned aspects.

3.1 Mechanics

The main body of the μ AUV² consists of three parts:

- 2 hollow acrylic glass domes, one at the front of the system and one at the back. These two domes build the hull protecting the inner part of the AUV from water up to a depth of 2.5 m. Both domes are transparent to allow optical sensors to monitor the environment.
- 1 central base frame made of aluminium which connects the two acrylic domes. This frame also serves as a carrier for all three thrusters and the battery pack, see Figure 1, label H.

The AUV has the dimensions $270 \times 182 \times 156 \text{mm}^3$ (Lx-HxW).

3.1.1 Propulsion

3 thrusters are responsible for moving the μ AUV² in all directions. The top thrusters can be turned independently $\pm 90^\circ$. The two side thrusters can be synchronously turned $\pm 90^\circ$. All thrusters are propelled by Maxon RE 10 DC motors in a 6V/1.5W

configuration. In combination with the epicyclic 16:1 gear Maxon GP10a1 and the Maxon quadrature encoder MR S 16 they actuate the μ AUV². All three thrusters can be rotated by Krick micro pile gear motors whose current angle of rotation is measured with potentiometers (Schmid, 2008). The configuration and the high flexibility of the thrusters make the AUV highly agile compared to miniaturized AUVs in its class (see Section 2))

3.1.2 Buoyancy Tank

Like the CoCoRo system (see Section 2) the μ AUV² also contains a buoyancy tank. This buoyancy or ballast water tank enables the μ AUV² to float energy efficiently at a certain depth in the water column. The tank can be filled and emptied with a peristaltic pump. The ballast water tank itself is a simple convoluted rubber gaiter. To prevent an overfilled water tank, the status (full/not full) of the water tank is measured with an ordinary mini push-button switch. The fill level is determined by measuring the time the pump is switched on while the throughput of the peristaltic pump is known.

3.2 Electronics

The main electronics were designed with modularity and miniaturization in mind. It consists of 5 stackable PCBs (Printed Circuit Boards) named Microcon 1, 2, 3, 4 and 5 respectively. All PCBs have the same form factor and are thus stackable. This concept enables an easy extension by further electronic components if needed. Microcon1 is responsible for driving the motors, generating the system voltage and for determining the motor current. The second board contains the communication hardware: 4 UARTs for serial communication, 8 GPIOs and in addition 3 eight channel ADCs. Microcon3 is the processing board. It embeds a Xilinx Virtex 4 FPGA (XC4VLX25) with an 8Mbit configuration Flash and 512k x 8 bit low voltage SRAM. Microcon4 houses a Blackfin DSP, static memory and flash memory. Microcon5 houses a camera (see Section 3.2.1) and the corresponding electronics. All PCBs offer a small form factor of only 35x80mm.

The μ AUV² contains several complementary sensors to control the thrusters and to navigate autonomously under water.

3.2.1 Camera

For environmental perception the μ AUV² is equipped with two ON Semiconductor MT9V022 digital cameras, one pointing downward and one pointing ahead.

With a wide VGA resolution (752Hx480V), global shutter, a frame rate of 60fps and optional 8 bit serial (LVDS) or 10 bit parallel video data output, the camera is ideal for machine vision tasks. Being connected to an FPGA, the machine vision algorithms can be accelerated with minimum power consumption compared to CPU or GPU computation.

3.2.2 IMU

To measure the attitude of the vehicle, an Inertial Measurement Unit (IMU) was developed. The μ IMU has a size of 20x20x20mm and consists of 1 gyroscope per axis, a three-axis acceleration sensor and a three-axis magnetometer. An on-board controller filters and fuses the sensor values with a Kalman filter (Kalman, 1960) and calculates the quaternions to determine the actual attitude of the system. The data is sent to the central processing unit via UART.

3.2.3 Differential Pressure Sensor

The differential pressure sensor Freescale MPX5100DP is used to determine the depth of the vehicle. With a sensitivity of 45mV/kPa and a range from 0 to 100kPa the sensor will deliver 4.5mV/cm. The 12 bit ADC which transforms the analog output into the digital domain has a resolution of 240 μ V/bit leading to a depth resolution of 1.8mm per bit.

3.2.4 Thruster Attitude Sensor

The current inclination of the thrusters can be measured by potentiometers (Piher N15TV) which are mounted on the turning axis. Linear potentiometers change their voltage division ratio proportional to the angle of rotation of the shaft of the potentiometer. Using an analog to digital converter (ADC) the output voltage of the potentiometer can be converted into the digital domain. Thus the determined inclination of the thrusters is used for control.

3.2.5 Thruster and Pump Speed Sensors

The speed of the thruster and pump motors is measured with quadrature encoders.

As already mentioned in Section 3.1.1, the used quadrature encoder is a Maxon MR S 16. The sensor delivers 16 counts per turn and in combination with the used 16:1 Maxon gear, 256 counts are produced for one 360° shaft revolution. Maximum electrical and mechanical speeds are 3000rpm.

3.2.6 Communication Module

Underwater wireless communication is still an area of research. Depending on the transmission power, high speed communication methods like WLAN or Bluetooth usually last less than 10cm. This is because the attenuation of frequencies in the range of radio waves in water is very high compared to the attenuation in air due to the dipole nature of the water molecules (Bryant, 2002). Long range communication channels like Long Baseline Modems (LBLs) are too bulky for a miniaturized AUV and due to their low frequency range acoustic methods do not have the capability to transmit a huge amount of data in an appropriate time.

In contrast, optical communication methods provide a throughput which is high for certain wavelengths. A very low attenuation ($2 \cdot 10^{-2}/m$) appears for a wavelength of $480nm$. Thus the μAUV^2 is equipped with an optical communication module that was developed at the DFKI. This means of communication was also chosen because the range that is covered by optical underwater communication modules easily covers the dimensions of the basin that is available for tests at the DFKI GmbH. Data is sent with a green (530nm) LED. An OTS IrDa (infrared data) transceiver (Maxim Integrated MAX3120) physical layer is used for controlling the LEDs. The complete OptCom module is UART compatible and fits on one of the PCBs mentioned in section 3.2. The data rate achieved is 19.2kbps with a range of approximately 2.5m.

4 SYSTEM PARAMETER IDENTIFICATION

The system model introduced by (Fossen, 2002) builds the basis for the controller. The identification process of the corresponding model parameters as described in (Indiveri, 1998) and (Ridao et al., 2001) is described in this Section.

4.1 Pressure Sensor

The diving depth of an underwater vehicle can be calculated by Equation 1, where p is the hydrostatic pressure [Pa], h is the depth in meter, ρ is the density of water [kg/m^3] and g is the gravitational acceleration ($9.81 m/s^2$).

$$p = h\rho g \quad (1)$$

The pressure sensor provides information about the current pressure surrounding the AUV. Equation

2 is used to convert sensor output data into depth information,

$$d(V) = C_1V + C_2 \quad (2)$$

where $d(V)$ is the depth, V is the output voltage of the sensor, C_1 is a constant factor and C_2 is an offset. For identifying the constants C_1 and C_2 , the μAUV^2 is manually submerged to a depth of 50cm which is the maximum depth of the available pool. The system was then ascended in steps of 5cm.

We used linear regression to identify the constants (see Table 1 and Figure 2).

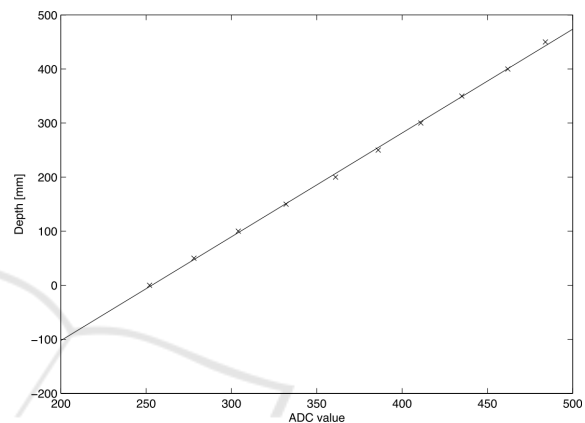


Figure 2: The sampled pressure sensor output data with linear regression (Schmid, 2008).

Table 1: Results of the system identification of the pressure sensor.

C_1	1.920m/V
C_2	-486.4mm
R^2 static	0.993

4.2 Thrusters

The following one-state thruster model was proposed by (Yoerger and Slotine, 1991)

$$\tau = C_t n |n| \quad (3)$$

$$\dot{n} = \beta T - \alpha n |n| \quad (4)$$

where τ is the output force, C_t , α and β are system constants, n is the propeller revolution rate and T is the input torque. Due to the usage of small and lightweight propellers, the time constant of the thrusters is assumed to be very small compared to the time constant of the system. Therefore the thruster dynamics can be neglected. C_t varies depending on the sign of the revolution rate (forward/backward) and is thus denoted as C_t^+ and C_t^- . The experimental setup to identify the thruster force parameters is depicted in Figure 3. The μAUV^2 is in the middle of the pool while it is attached to an aluminium rod. Outside of

the pool is a scale on which the μ AUV² generates a force when the thrusters are turned on. This is due to a mechanical connection between the AUV and the scale via a lever arm.

The speed of the side thrusters is increased synchronously from -100% to $+100\%$ in steps of 5% while the related weight on the scale is saved. The torque that is generated in point O by the force of the two side thrusters can be calculated using Equation 5.

$$\tau_O = 2f_t d_t \quad (5)$$

τ_O is the torque in point O , f_t is the thrust of one thruster and d_t is the perpendicular distance of the thrusters from O . On the scale a force f_s is induced by the torque τ_O which can be determined by equation 6

$$\tau_O = m_s g d_s \quad (6)$$

where m_s is the measured weight on the scale, g is the gravitational constant and d_s is the length of the arm between O and the point of contact on the scale. Using Equations 5 and 6, the resulting thruster force can be calculated as

$$f_t = \frac{d_s}{2d_t} m_s g \quad (7)$$

With $f_t = \tau$ from Equation 3 we find

$$\frac{d_s}{2d_t} m_s g = C_t n |n| \quad (8)$$

Linear regression on the measured (m_s, n) tuples (see Figure 4) reveals the parameter C_t^\pm .

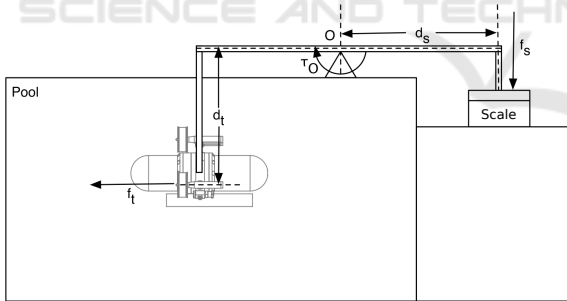


Figure 3: Thruster force identification experiment set-up (Schmid, 2008).

Table 2: Results of the experiments with the thrusters.

C_t^+	$13.2 \cdot 10^{-06} Nm (\frac{s}{U})^2$
C_t^-	$-8.32 \cdot 10^{-06} Nm (\frac{s}{U})^2$
R^{2+} static	0.9990
R^{2-} static	0.9989

4.3 Damping Coefficient

The motion of a moving, submerged object is damped by friction generated by the surrounding liquid particles (Fossen, 2002). The following assumptions are

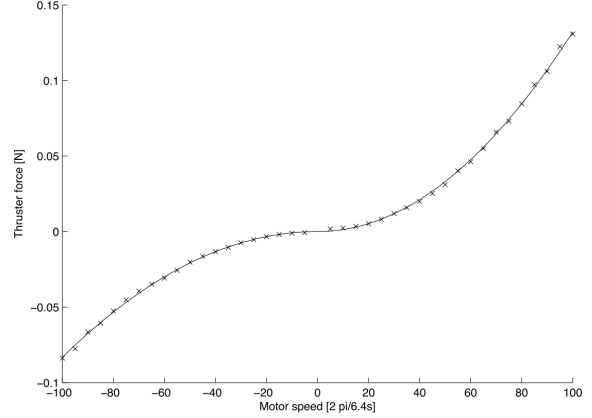


Figure 4: Thruster force over revolution rate including linear regression (Schmid, 2008).

made to reduce the complexity such that the damping coefficients can be determined experimentally.

1. Only steady state movements without linear accelerations are considered
2. Only linear movements are considered
3. The AUV is stable with zero buoyancy and no roll and pitch are assumed
4. In contrast to the definition by (Fossen, 2002) where D is a complex function depending on v , we use the approximation of (Leonessa, 2008) in Equation 9 for linear and quadratic damping (Christensen et al., 2009).

$v = [u \ v \ w \ p \ q \ r]^T$ represents the position in a body fixed system $\{B_{xyz}\}$ in all 6 degrees of freedom.

$$D = -diag(X_u, Y_v, Z_w, K_p, M_q, N_r) \\ D(v) = -diag(X_u|u|, Y_v|v|, Z_w|w|, K_p|p|, M_q|q|, N_r|r|) \quad (9)$$

$$D(v)v = \tau$$

$$= \begin{pmatrix} X \\ Y \\ Z \\ K \\ M \\ N \end{pmatrix} = \begin{bmatrix} X_u & 0 & 0 & 0 & 0 & 0 \\ 0 & Y_v & 0 & 0 & 0 & 0 \\ 0 & 0 & Z_w & 0 & 0 & 0 \\ 0 & 0 & 0 & K_p & 0 & 0 \\ 0 & 0 & 0 & 0 & M_q & 0 \\ 0 & 0 & 0 & 0 & 0 & N_r \end{bmatrix} \begin{pmatrix} u \\ v \\ w \\ p \\ q \\ r \end{pmatrix} + \begin{bmatrix} X_{u|u|}|u| & 0 & 0 & 0 & 0 & 0 \\ 0 & Y_{v|v|}|v| & 0 & 0 & 0 & 0 \\ 0 & 0 & Z_{w|w|}|w| & 0 & 0 & 0 \\ 0 & 0 & 0 & K_{p|p|}|p| & 0 & 0 \\ 0 & 0 & 0 & 0 & M_{q|q|}|q| & 0 \\ 0 & 0 & 0 & 0 & 0 & N_{r|r|}|r| \end{bmatrix} \begin{pmatrix} u \\ v \\ w \\ p \\ q \\ r \end{pmatrix} \quad (10)$$

$X_u, Y_v, Z_w, K_p, M_q, N_r$ are linear and $X_{u|u|}|u|, Y_{v|v|}|v|, Z_{w|w|}|w|, K_{p|p|}|p|, M_{q|q|}|q|, N_{r|r|}|r|$

are quadratic damping factors. Under the mentioned assumptions the six degrees of freedom can be separated such that each degree of freedom is an equation of the form

$$D_v v_{max} + D_{v|v}|v_{max}|v_{max}| = \tau \quad (11)$$

with v_{max} as the constant maximum velocity at an input force/torque of τ . Because only heave and yaw will be controlled actively in a closed loop configuration, the only parameters that need to be identified to determine suitable controller parameters are Z_w , $Z_w|w|$, N_r and $N_r|r|$.

The experimental setup for the identification of the heave parameters was as follows: The μ AUV² was submerged to the bottom of the pool. Then it emerged with a constant thruster force which was varied in subsequent experiment runs. The diving speed is determined by the derivation of the pressure sensor data. The (w_{max}, Z) tuples are the sampling data for a linear regression on Equation 11. The heave position was measured with varying values for $Z = [0.0238 \ 0.0324 \ 0.0423 \ 0.0535 \ 0.0661 \ 0.08 \ 0.0952 \ 0.1117 \ 0.1295]N$. Figure 5 shows the result of the regression and the maximum reachable heave speed over the applied force. The results can be seen in Table 3.

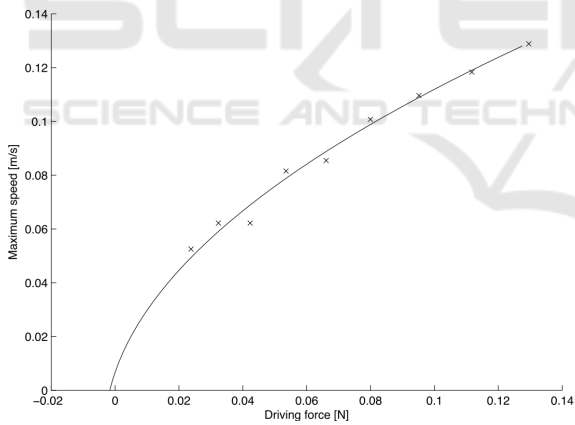


Figure 5: Maximum heave speed over driving force ((Schmid, 2008)).

To identify the yaw damping, the experimental setup starts with positioning the μ AUV² in the middle of the pool. Then a defined and constant torque is applied to both side thrusters. The torque is varied with each consecutive run of the experiment. The yaw turning speed is logged from the IMU. Different yaw speeds were measured for the corresponding torques $\tau = [0.0013 \ 0.0020 \ 0.0027 \ 0.0033 \ 0.0040 \ 0.0047 \ 0.0053]Nm$.

Figure 6 shows the resulting regression function and the measured maximum yaw speed samples.

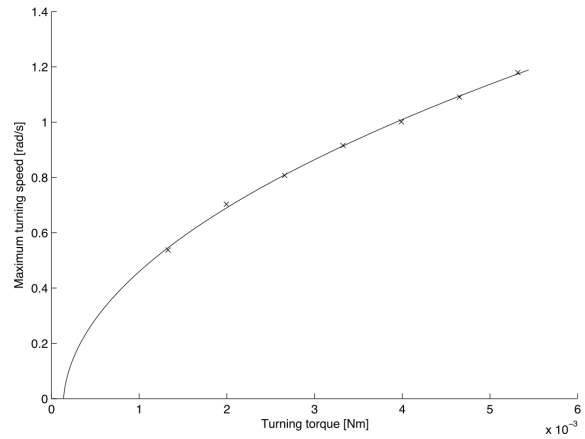


Figure 6: Maximum yaw speed over driving force with regression function ((Schmid, 2008)).

The results of the experiments are summarized in Table 3.

Table 3: Results of the damping experiments.

Z_w	$204 \cdot 10^{-3} \frac{Ns}{m}$
$Z_w w $	$6.28 \frac{Ns}{m}$
ZR^2 static	0.9902
N_r	$251 \cdot 10^{-6} \frac{Ns}{m}$
$N_r r $	$3.54 \cdot 10^{-3} \frac{Ns}{m}$
NR^2 static	0.9990

4.4 Additive Mass

In this section, the added mass of the vehicle is estimated. The added mass is an extra virtual mass term, since an accelerating or decelerating body must move some volume of the surrounding fluid as it moves through it (Fossen, 2002).

If we assume that:

1. The vehicle is accelerating such that $\dot{v} \neq 0$
2. The movement of the AUV is linear along one axis
3. Buoyancy, roll and pitch are zero

the system equation from (Fossen, 2002) can be simplified to

$$\tau - D(v)v = (M_{RB} + M_A)\dot{v} \quad (12)$$

with $M_{RB} + M_A = M$ (M_{RB} = mass of the rigid body and M_A =additive mass) being the only parameter, because the damping coefficients were already identified in Section 4.3. τ are the forces/torques in a body fixed system $\{B_{xyz}\}$. The degrees of freedom in Equation 12 are assumed to be separable resulting in Equation 13

$$\tau - D(v)v - D_{v|v}|v|v| = M\dot{v} \quad (13)$$

The total effective mass parameter M can be identified with a linear regression on Equation 13 and the data tuples $(\tau - D(v)v - D_{v|v}|v|\dot{v})$. Measurements show that the above mentioned condition $\dot{v} \neq 0$ is true between $t = 1.5s$ and $t = 3s$. Figure 7 shows the fitted regression result with the regression input data tuples. Table 4 lists the regression results.

Identifying the effective mass for heave is more critical than for yaw because the current depth is the only measurable system state and Equation 13 needs the first and second derivative of the depth. The IMU acceleration sensors do not permit to detect small changes in acceleration due to a low resolution and noisy signals of the sensors. Therefore, the second derivative needs to be determined numerically which is badly conditioned as high frequency noise is amplified. Measurements showed that the acceleration phase is between $t = 2.5s$ and $t = 3.5s$. A regression line through the data tuples can be seen in Figure 8. The coefficient of determination R^2 is very bad with a value of 0.80.

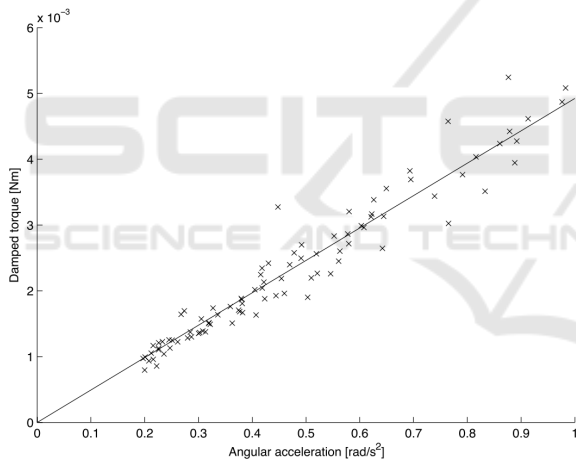


Figure 7: Damped yaw torque over acceleration ((Schmid, 2008)).

Table 4: Additive mass parameters.

I_{zz}	$4.9 \cdot 10^{-3} kg \cdot m^2$
$I_{zz}R^2$ static	0.9990
m_z	1.96kg
m_zR^2 static	0.80

5 SYSTEM CONTROL

The system model and the identified parameters are the basis for the layout of the controller system. This section will begin with defining the system properties. Then the controller structure will be explained in de-

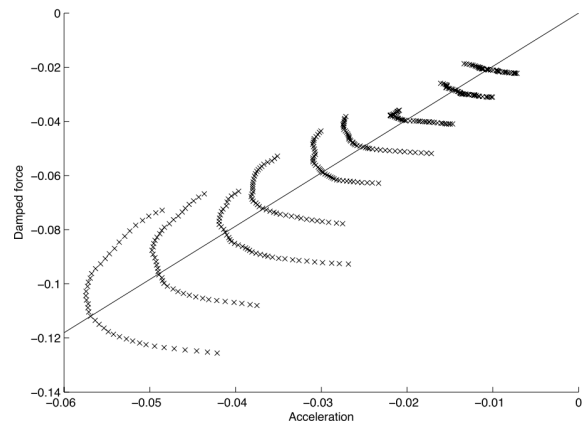


Figure 8: Damped heave force over acceleration ((Schmid, 2008)).

tail providing both information about the simulation and information about the implemented controller.

5.1 μ AUV² System Properties

Tests showed that the μ AUV² is stable concerning roll and pitch as long as the thruster controllers only generate low frequency thruster angle changes. Thus both roll and pitch are controlled passively. In the following the angles α and β are related to the orientation of the top- and side thrusters respectively. The following modes were defined to control the μ AUV² :

1. Diving mode, $\alpha = 0, \beta = -\pi/2$. Top thruster turned off. Used for pure heave control
2. Buoyancy mode: diving with pump control
3. Turning mode: $\alpha = 0, \beta = 0$ Top thruster turned off. Used for pure yaw control
4. Drift mode: $\alpha = \pi/2, \beta = 0$. Top thruster turned off. Used for pure yaw control
5. Auto mode: $\alpha = 0, \beta \in [-\pi/4; \pi/4]$. Used for concurrent heave, yaw and surge control

5.2 Controller Structure

We first designed a simulation to test the AUV controllers: Figure 9 shows the block diagram of the simulated control system.

Inputs are in absolute values for heave and yaw in $\{W_{xyz}\}$, desired thruster forces for surge and sway in $\{B_{xyq}\}$ and the mode of the controller. The block labeled CTRL1 is the implementation of the controller. It will be described in detail in this paragraph. Controller output thrust is limited by the saturation block to the maximum thrust of the used thrusters. A moving average lowpass filter is used to suppress fast thruster movements related to the fast changes in the

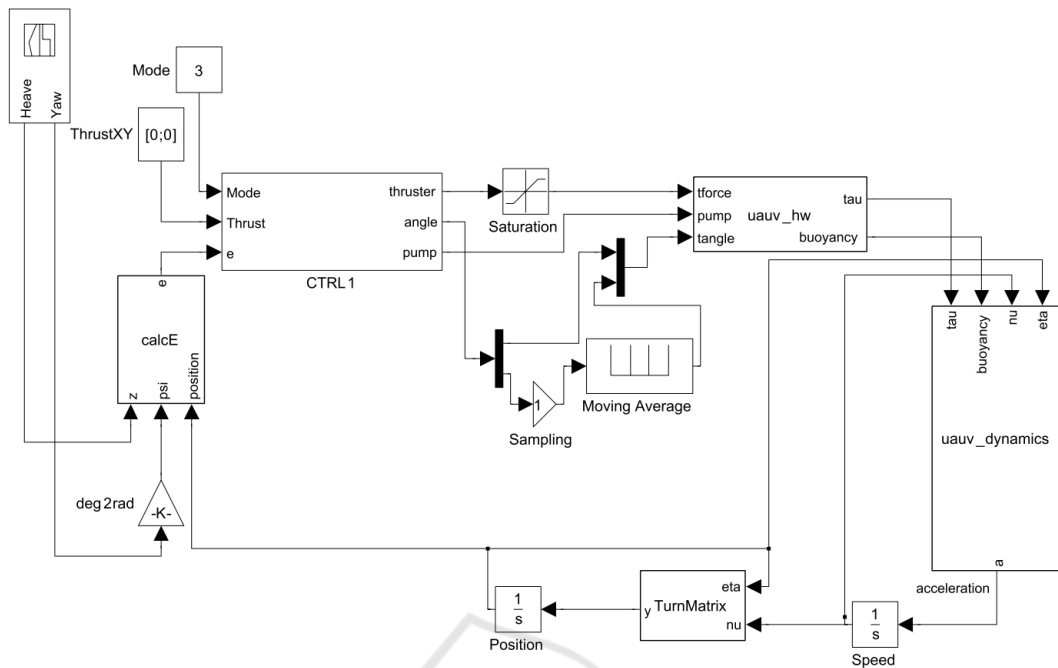


Figure 9: Block diagram of the complete control system ((Schmid, 2008)). Inputs are on the left and outputs are on the right.

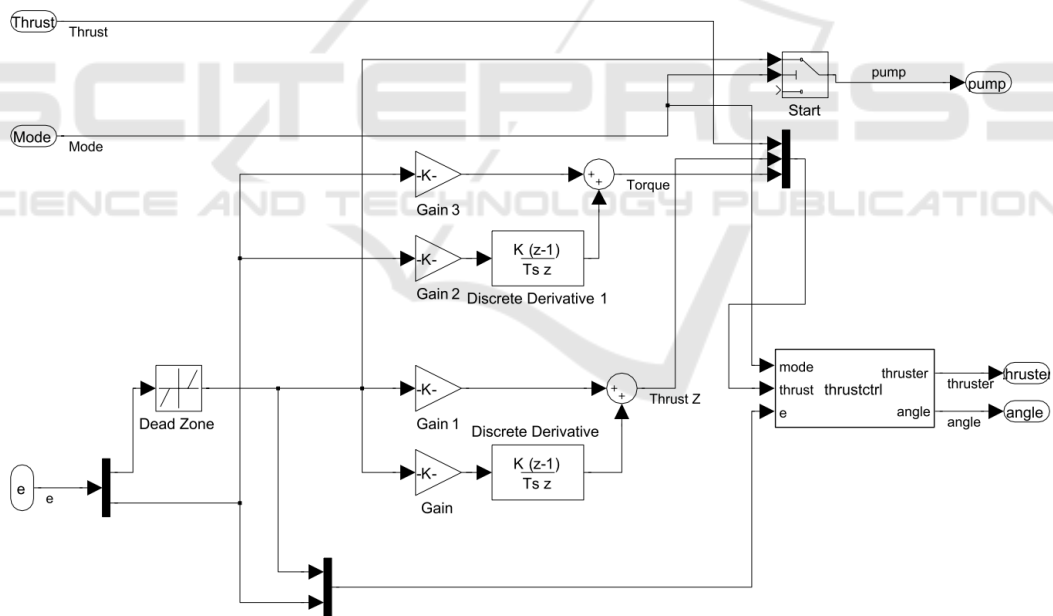


Figure 10: Detailed CTRL1 block diagram (Schmid, 2008).

output of the related controller because these might destabilize the μAUV^2 . The block labeled *uauv_hw* transforms thruster force to applied force in $\{B_{xyq}\}$. In addition it is responsible for controlling the buoyancy state. The system equation from (Fossen, 2002) is modeled in block *uauv_dynamics* to determine the system acceleration against the current system states. To get the system speed the acceleration state is inte-

grated over time. This value is fed back to the system dynamic block. A transformation matrix is used to transform the system speed from $\{B_{xyq}\}$ to $\{W_{xyq}\}$. This speed vector is integrated to determine the position of the system. The resulting value is fed back to both the turning matrix and the AUV dynamics block. To calculate the heave and yaw controller error the position is used. Please keep in mind that the system

only implements the actively controlled DOF.

Figure 10 shows a detailed block diagram of the implemented controller block CTRL1. The error inputs for heave and yaw are used as inputs for two PD controllers. A heuristic method was used to estimate the values for P- and D in simulation. Fine tuning of the parameters was done in the water basin. Depending on the controller mode, the PD controller outputs as well as the rest of the CTRL1 block inputs are used for thrust and angle calculation. In buoyancy mode, a bang-bang controller was used for the pump with a dead zone on the heave error.

5.3 RESULTS

A minuscule AUV named μ AUV² has been technically described in this paper. The system was successfully tested in waterbasins at the DFKI GmbH in Bremen, Germany. System parameters have been identified experimentally. They have been the basis for the controller design. This section presents the main simulation and experimental results.

5.4 Diving Control

To analyse the performance of the diving controller, a diving trajectory was defined. Starting at the surface of the water, a new depth value of 0.4m is set after $t=10s$. 15s later the value is changed to 0.2m. At $t=40s$ the depth is set to 0m.

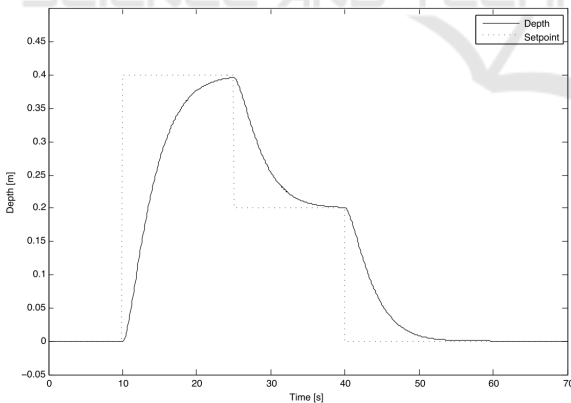


Figure 11: Diving controller in simulation (Schmid, 2008).

The trajectory was used for simulation (Figure 12) and real runs (Figure 12). In simulation the system shows no overshoot for $\omega_z = 0.6$ as $\zeta_z = 1$. The system successfully reaches the setpoints after 15s. In reality the system reacts much faster. Setpoints are reached after 7s. The determined error of 8mm is very low.

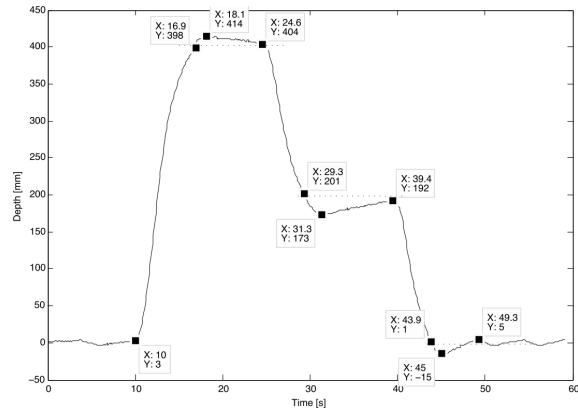


Figure 12: Diving controller on a real run (Schmid, 2008).

5.5 Buoyancy Control

A buoyancy calibration run before each system start is crucial because the depth controller is designed for zero buoyancy.

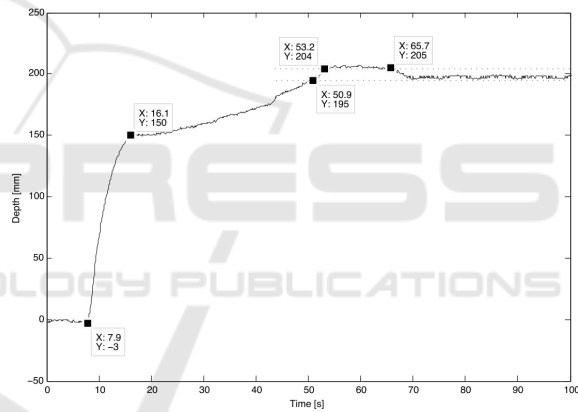


Figure 13: Buoyancy compensation run (Schmid, 2008).

The calibration can be seen in Figure 13. It starts by setting the depth to 0.2m while the μ AUV² has a positive buoyancy. A depth of 0.15m is reached after 16s. The PD controller has a steady state error of 0.05m. After 51s the pump has reduced buoyancy so much that the dead zone is reached. 2s later the dead zone is left again because a negative buoyancy was reached. The system reacts by increasing the buoyancy such that the system re-enters the dead zone. Now a zero buoyancy state is reached.

The control effort was chosen low ($\omega_z = 0.4$) on purpose to avoid large overshoots which could even lead to oscillations. Once the dead zone is reached the system stays in the dead zone of 8mm for at least 30s.

5.6 Turning Control

Again a trajectory was defined to evaluate the turning control mode.

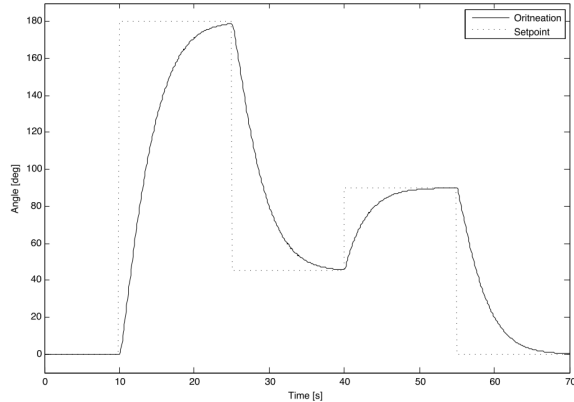


Figure 14: Simulation results of the turn controller (Schmid, 2008).

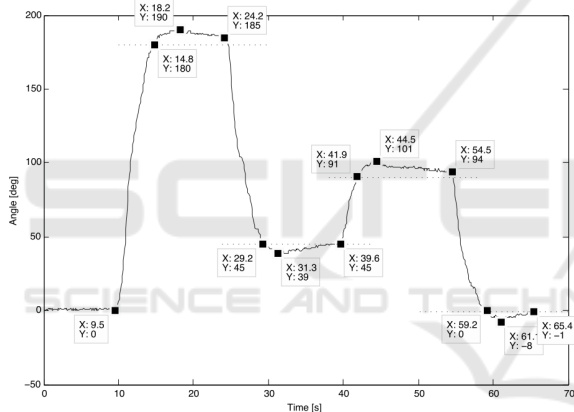


Figure 15: Turning control with $\omega_{\psi} = 0.6$ and increased $K_{D\psi} = 0.016$ (Schmid, 2008).

The simulation can be seen in figure 14. It starts at an orientation of 0° . After 10s, the set point becomes 180° , 15s later it is set to 45° for 15s to jump to 90° at a time of 40s. At 55s the orientation is reset to 0° . To reduce overshoots the $K_{D\psi}$ part was increased. The maximum overshoot is 10° which corresponds to 2.8% of the total angle range of 360° . The controller reaches a maximum average turning speed of $34^\circ/s$ which is about 60% of the maximum possible turning speed of the μAUV^2 (see Figure 15).

5.7 Auto Mode Control

To compare both the diving and turning controllers with the auto mode controller the same trajectories mentioned in the corresponding sections were created for the auto mode controller. Surge and sway mo-

tion should be suppressed by the controller. The side thruster angle does not permit high frequency movements (except for the steps at a set point change which is acceptable). Surge and sway stayed at zero for the whole simulation time. The top thruster could perfectly compensate the surge force of the two side thrusters. In reality, the auto heave controller is a lot slower than the diving controller, see Figure 16.

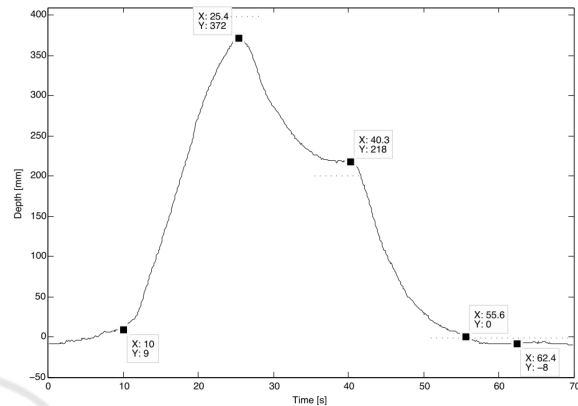


Figure 16: Performance of the auto mode controller, heave (Schmid, 2008).

The maximum average speed of $0.0024m/s$ is less than the half of the depth control performance. The effect can be explained with the thruster saturation. The total surge force that is produced by the side thrusters is limited to the maximum thrust level that the top thruster can produce to compensate the surge motion and stay at the same place. This also reduces the thrust that is used for diving. It can also be seen that overshoots mentioned before disappeared and a steady state error of a maximum of $0.018m$ could be reached. In relation to the total pool depth of $0.6m$, the error is still acceptable.

The maximum average turning speed is only slightly reduced to $28^\circ/s$ (compared to $34^\circ/s$ in turning mode), see Figure 17. The overshoot rates are also similar to the diving mode. This result was expected as the turning force is prioritized when the total side thruster force is calculated. Another effect that can be seen is the oscillation of the yaw angle. A possible reason might be water turbulence that is produced by the different turning directions of the side thrusters and the top thruster. It should be mentioned that the system did not exactly stay at the original surge and sway position in contrast to simulations. This might also be caused by non linear turbulence effects that were not considered. Without an exact knowledge of the actual position in surge and sway it would not be possible to control the system and prevent this movement.

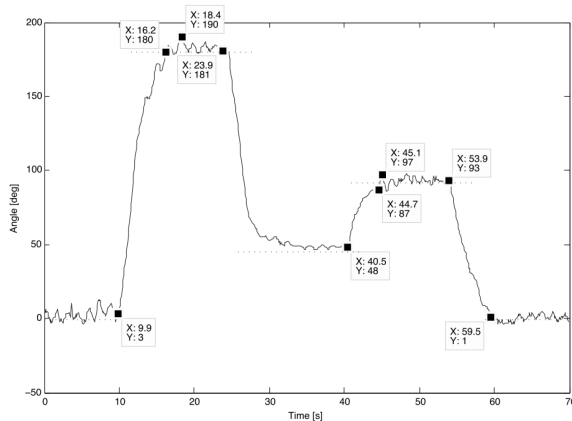


Figure 17: Performance of the auto mode controller, yaw (Schmid, 2008).

6 DISCUSSION

6.1 System Design

The mechanical part of the μ AUV² has proven to be very robust and the propulsion system has sufficient power to propel the system. One drawback of the thrusters is the fact that the thrusters have an insufficient sealing concept. This leads to the problem that over time water accumulates in the inside of the thrusters. An ideal solution for hovering in the water column is the use of a buoyancy tank. All sensors fulfill their requirements and especially the IMU which outputs quaternions, even though there is a need for a more accurate acceleration, speed and position values. Being extendable and providing a lot of computational power makes the μ AUV² an ideal platform for the purposes mentioned in section 1. Communication via an optical link has proven to be very robust even though the data rate should be increased in the future. A very useful feature is the possibility to program the system when it is fully assembled.

6.2 Identification of System Parameters

The presented simplified model is a good start but can be improved in the future. It is used as a first pass attempt and the results are still useful for control. The correlated errors in Figure 8 imply an error, where regression fails. The bad conditioning cannot be fully explained by high frequency noise as hypothesised. Regression may try to average out the errors, but the R^2 metric and the method itself expects white noise, uncorrelated errors. Assuming that the total mass is constant leads to a modelling error. The thrust modelling might be too simplistic for the dynamic case

because static thrust does not equal dynamic thrust. This also impacts the thrust vs. damping force results. Another cause could be laminar flow in all directions except for the heave direction where turbulent flow might dominate due to the non-streamline battery pack.

6.3 Controller

The simulated controller has proven to work in the real system. A major problem is the lag of position information in surge and sway and imprecise position, speed and acceleration data.

One of the reasons for the gap between simulation and reality (see Section 5.4) is the simplified system model used throughout this paper. Other possible reasons could be an inaccuracy in the experiments (see Section 4) or the fully charged battery pack which might lead to a motor speed slightly over the theoretical speed.

7 CONCLUSION AND FUTURE WORK

This paper has presented a minuscule AUV named μ AUV². As soon as basic autonomous behavior is implemented, the μ AUV² could be tested in outside watercourses. Its behavior in water currents would shed light on the feasibility of the application of μ AUV² in open water. It would also be very interesting to implement a controller for the μ AUV² to do a roll or a loop around the y-axis. The thrusters would have to produce a sinusoidal force with the resonance frequency of the system on the corresponding axis. In any case, there are a lot of conceivable functions that could be implemented in the future.

An interface for easily equipping the μ AUV² with new sensors could accelerate many tasks. Hull improvements are mainly focused on the thrusters and the battery pack. The thrusters are the weak point in the design concerning maximum dive depth. Due to the thruster design, the dive depth is currently limited to approximately 2m. This together with the fact that water accumulates in the thrusters will make a redesign of the thrusters necessary. A possible improvement could be a magnetically coupled thruster. A further step towards a streamlined hull will require a redesign of the battery pack,

A major problem of the controller, the lag of position information in surge and sway, could be solved with the camera on the bottom. An algorithm for optical flow could be implemented to calculate the actual moving speed. Furthermore, the absolute posi-

tion could be calculated by integrating the speed. Additionally, optical markers on the ground of the pool further improve the position estimate. The second camera might be used for obstacle detection. With this additional sensor information it would be possible to create a map of the area the AUV is moving in.

As said before, the presented simplified model is a good start. But e.g. the error in Figure 8, implies that the system model can be improved.

ACKNOWLEDGEMENTS

The project DAEDALUS is funded by the German Space Agency (DLR, Grant number: 50NA1312) with federal funds of the Federal Ministry of Economics and Technology (BMWi) in accordance with the Bundestag resolution of the German Parliament.

REFERENCES

- Albiez, J., Gaudig, C., Hilljegerdes, J., and Kirchner, F. (2015). FlatFish A compact subsea-resident inspection AUV. *Unknown*, 1(November).
- Barngrover, C., Kastner, R., Denewiler, T., and Mills, G. (2011). The stingray auv: A small and cost-effective solution for ecological monitoring. In *OCEANS 2011*, pages 1–8.
- Bryant, S. (2002). Ice-embedded transceivers for europa cryobot communications. *IEEE Aerospace Conference Proceedings*, 1(1):349–356.
- Christensen, L., Kampmann, P., Hildebrandt, M., Albiez, J., and Kirchner, F. (2009). Hardware rov simulation facility for the evaluation of novel underwater manipulation techniques. In *OCEANS 2009 - EUROPE*, pages 1–8.
- Dowdeswell, J., Evans, J., Mugford, R., Griffiths, G., McPhail, S., Millard, N., Stevenson, P., Brandon, M., Banks, C., Heywood, K., Price, M., Dodd, P., Jenkins, A., Nicholls, K., Hayes, D., Abrahamsen, E., Tyler, P., Bett, B., Jones, D., Wadhams, P., Wilkinson, J., Stansfield, K., and Ackley, S. (2008). Instruments and methods autonomous underwater vehicles (auvs) and investigations of the ice/ocean interface in antarctic and arctic waters. *Journal of Glaciology*, 54(187):661–672.
- Fechner, S., Kerdels, J., Albiez, J., and Kirchner, F. (2007). Design of a uauv. In *Autonomous Minirobots for Research and Edutainment (AMiRE-2007). Proceedings of the 4th International AMiRE Symposium (AMiRE-2007)*, Heinz Nixdorf Institut Universit Paderborn, pages 99–106.
- Fossen, T. I. (2002). *Marine control systems: guidance, navigation and control of ships, rigs and underwater vehicles*. Marine Cybernetics AS.
- Indiveri, G. (1998). Modelling and identification of underwater robotic systems. *Computer Science*.
- Kalman, R. E. (1960). A new approach to linear filtering and prediction problems. *Transactions of the ASME—Journal of Basic Engineering*, 82(Series D):35–45.
- Leonessa, A. (2008). Underwater robots: Motion and force control of vehicle-manipulator systems (g. antonelli; 2006) [book review]. *IEEE Control Systems*, 28(5):138–139.
- Meyer, B., Ehlers, K., Isokeit, C., and Maehle, E. (2014). The development of the modular hard- and software architecture of the autonomous underwater vehicle monsun. In *ISR/Robotik 2014; 41st International Symposium on Robotics; Proceedings of*, pages 1–6.
- Mintchev, S., Donati, E., Marrazza, S., and Stefanini, C. (2014). Mechatronic design of a miniature underwater robot for swarm operations. In *Robotics and Automation (ICRA), 2014 IEEE International Conference on*, pages 2938–2943.
- Nicholson, J. and Healey, A. (2008). The present state of autonomous underwater vehicle (auv) applications and technologies. *Marine Technology Society Journal*, 42(1):44–51.
- Ridao, P., Batlle, J., and Carreras, M. (2001). Model identification of a low-speed uuv. *IFAC Conference Control Applications in Marine Systems, Glasgow, Scotland*.
- Schmid, K. (2008). *Embedded system and controller design for a micro AUV Diploma thesis*. Thesis, University of Bremen, TU Hamburg Harburg. https://www.researchgate.net/publication/299283880_Embedded_system_and_controller_design_for_a_micro_AUV.
- Yoerger, D. and Slotine, J.-J. (1991). Adaptive sliding control of an experimental underwater vehicle. In *Robotics and Automation, 1991. Proceedings., 1991 IEEE International Conference on*, pages 2746–2751 vol.3.